JOURNAL OF PETROLOGY | VOLUME 46 | NUMBER 2 | PAGES 275–290 | 2005 | doi:10.1093/petrology/egh071

Vapor-Absent Melting of Tonalite at 15–32 kbar

ALBERTO E. PATIÑO DOUCE*

DEPARTMENT OF GEOLOGY, UNIVERSITY OF GEORGIA, ATHENS, GA 30602, USA

RECEIVED OCTOBER 15, 2003; ACCEPTED AUGUST 6, 2004
ADVANCE ACCESS PUBLICATION OCTOBER 1, 2004

The behavior of igneous continental crust during subduction is modeled by means of vapor-absent partial melting experiments on a tonalite, containing equal amounts of biotite and hornblende, at pressures of 15–32 kbar. The experiments produce leucogranitic melts coexisting with garnet + omphacitic clinopyroxene + K-feldspar + kyanite + quartz/coesite ± phengite ± zoisite. Experimental constraints and geometrical analysis of phase equilibria show that the hydrous phases that control dehydration-melting of tonalites in deep thickened continental crust and in the upper mantle are phengite and zoisite. The negatively sloping amphibole + quartz vapor-absent solidus characteristic of amphibolites is largely suppressed in tonalites, because amphibole is eliminated by water-conserving reactions that also consume K-feldspar and kyanite and produce phengite and zoisite. The temperature at which melt first appears in the experiments varies from <900°C at 15 kbar, to 1000°C at 27 kbar, to <925°C at 32 kbar. Moderate degrees of partial melting (20–30%) yield residual assemblages with mantle-like densities but which can still contain minor amounts of hydrous phases. Partial melting of tonalitic crust during continental subduction can thus generate incompatible element-rich residues that would be able to remain in the mantle indefinitely, acting as long-term sources of metasomatic fluids.

KEY WORDS: *mantle; melting; metasomatism; tonalite; UHP metamorphism*

INTRODUCTION

Rocks of the upper continental crust are buried to depths in excess of 120 km during continental collisions (e.g. recent reviews by Ernst, 2001; Liou *et al.*, 2002; Chopin, 2003). Ever since continental subduction was first confirmed by the occurrence of coesite mineral inclusions in eclogites (Chopin, 1984; Smith, 1984), there have been considerable advances in our understanding of the metamorphic reactions that affect crustal rocks at ultrahigh pressure (UHP) conditions (e.g. Massonne, 1995, 1999; Liou *et al.*, 1998). Assemblages that are diagnostic of UHP metamorphism (UHPM) have been identified and mineral equilibria that can be used to estimate UHPM conditions quantitatively have been calibrated. Much of the interest has focused on identifying UHPM rocks at the surface of the Earth. In contrast, there has been relatively less discussion of the fate of crustal rocks during their mantle excursions. An important open question is whether there are instances in which crustal rocks fail to return from the mantle and what happens to them, and to the enclosing mantle, in those cases.

Many UHPM terranes appear to have undergone little or no partial melting at UHP conditions, although some degree of melting has taken place in some of these rocks (e.g. in the Kokchetav massif: Shatsky *et al.*, 1999; Hermann *et al.*, 2001; and in the Ezgebirge: Stöckhert *et al.*, 2001). Dearth of partial melting reflects the low geothermal gradients characteristic of ultrahigh pressure metamorphism (5–20°C/km, e.g. Chopin, 2003). Equally importantly, it also demonstrates that free H_2O-rich fluids are not normally present during continental subduction. If free aqueous fluids were present, then partial melting of quartzofeldspathic crustal lithologies would take place even under these depressed geothermal gradients (e.g. Chopin, 2003, fig. 1). Absence of partial melting in UHP rocks has an important implication that stems from the fact that if the rocks do not melt, then they are likely to preserve H_2O bound in hydrous minerals. Slices of supracrustal rocks that are trapped in the upper mantle could thus become important reservoirs of H_2O and incompatible trace elements. Such rocks may or may not eventually melt while they reside in the mantle, and they may or may not be able to remain in the mantle

*E-mail: klingon@3rdrock.gly.uga.edu

Table 1: Composition of starting material (wt %)

	SiO_2	Al_2O_3	TiO_2	FeO*	MgO	MnO	CaO	Na_2O	K_2O	F	Total
Plagioclase	61·40	24·11	n.d.	0·26	n.d.	n.d.	6·01	7·32	0·57	n.d.	99·69
K-feldspar	64·29	19·08	n.d.	0·09	n.d.	n.d.	0·20	1·86	13·56	n.d.	99·09
Biotite	38·26	15·55	2·68	14·60	14·42	0·17	0·06	0·41	9·12	1·52	96·79
Amphibole	47·48	7·12	1·02	15·65	12·31	0·61	11·93	1·02	0·64	0·08	97·84
Bulk rock	60·76	16·87	0·89	5·85	2·65	n.d.	5·33	3·83	2·54	n.d.	98·72
Whole crust[1]	57·26	15·87	0·90	9·08	5·30		7·39	3·10	1·09		100·0
Upper crust[1]	66·05	15·23	0·50	4·51	2·21		4·21	3·90	3·38		100·0

*Total Fe as FeO.
[1]Whole crust and upper crust compositions from Taylor (2001, table 12.5).

indefinitely. These are questions that have relevance to discussions of long-term changes in mantle compositions, mantle metasomatism and intracontinental magmatism. In order to address these questions, it is necessary to know the conditions at which vapor-free crustal rocks eventually melt at ultrahigh pressures, thus releasing their H_2O and incompatible elements.

The goal of this paper is to examine the UHP vapor-absent melting behavior of average upper-crustal igneous rocks. A calc-alkaline tonalite was chosen as representative of the average composition of upper continental crust of igneous origin. Some of the experimental results discussed here were previously reported in a preliminary fashion by Patiño Douce & McCarthy (1998, CAT starting material, at 15, 21 and 30 kbar). Additional experiments were completed, after the publication of that paper, at 18, 27 and 32 kbar. Full compositional data for all phases in all melt-bearing experiments at 15–32 kbar are given here for the first time.

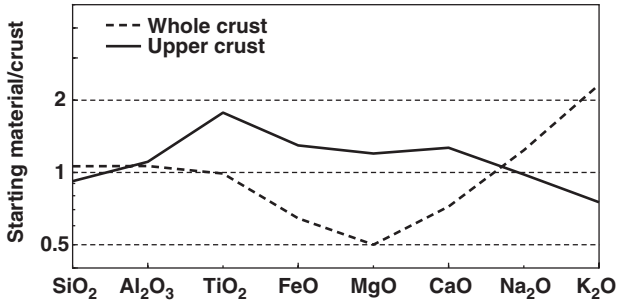

Fig. 1. Comparison of bulk composition of the tonalite starting material with whole continental crust and upper continental crust [data from Taylor (2001, table 12.5)].

EXPERIMENTAL AND ANALYTICAL PROCEDURES

Starting material

The starting material for all of the experiments was a calc-alkaline tonalite from the Sierra Nevada (California, USA), collected from Lee Vining Canyon. The rock is composed of plagioclase An_{30} (45%), quartz (20%), biotite (13%), hornblende (13%), K-feldspar (7%) and Fe–Ti oxides (2%). Bulk chemical composition and mineral compositions of the starting material are given in Table 1. The starting material is closer in composition to average upper continental crust than to average bulk continental crust [Table 1, Fig. 1; crustal data after Taylor (2001)]. Difference of the bulk analysis from 100 wt % (Table 1) suggests that the starting material may contain ~1·3 wt % H_2O. On the other hand, assuming that biotite contains 3·5 wt % H_2O and hornblende 2·5 wt % H_2O, the modal composition of the tonalite results in 0·8 wt % bulk H_2O-content. I will use an intermediate value of 1 wt % as a rough estimate of the H_2O-content of the tonalite.

Sample preparation and containment

The starting material was ground for 1 h in a shatter box with WC lining and balls, in order to attain a grain size ≤10 μm. Samples (approximately 3 mg) were contained in welded Au capsules with 1·0 mm inner diameter and 0·2 mm wall. The capsules were loaded and then stored open in an oven at 130°C for at least 24 h, in order to eliminate adsorbed humidity. The capsules were crimped inside the oven and immediately sealed by arc welding.

Experimental apparatus

All experiments were performed in a solid-medium piston-cylinder apparatus at the University of Georgia, with 0·5 inch diameter NaCl–graphite cell assemblies. Experiments were run at pressures of 15–32 kbar and temperatures of 900–1150°C, with run durations varying

Table 2: Run conditions, phase assemblages and modal compositions (wt %)

Run number	*P* (kbar)	*T* (°C)	Time (h)	Qtz	Kfs	Plg	Ky	Grt	Cpx	Bt	Phn	Zo	Rt	Glass
TED 53	15	900	198	X	X	X		X	X	X			X	tr
APD 651	15	950	175	11·4	13·3	27·6		18·2	9·2	2·2			X	18·1
APD-665	18	900	202	unmolten										
TED 51	21	940	189	13·2	31·4		6·0	17·6	21·6				X	10·2
TED 50	21	960	187	11·2	29·5		4·5	20·8	21·6				X	12·4
TED 47	21	975	175	9·4	27·8		3·5	22·0	21·4				X	15·9
TED 44	21	1025	150	6·5	20·2		3·0	21·3	16·3				X	32·7
TED 52	21	1060	132		11·8			20·7	13·0				X	54·5
FCH-5	27	1000	118	unmolten										
APD-683	27	1025	149	18·9	14·6		1·5	16·6	30·3		4·5	5·3		8·3
APD-682	27	1075	126	11·4	12·3		0·9	17·3	30·5		1·8	3·5		22·3
FCH-9	27	1100	118	9·2	12·6		1·4	18·0	29·5			2·8		26·4
APD-685	27	1125	78	6·7	8·4		1·5	19·9	24·3					39·2
APD-684	27	1150	53	9·9		9·9	1·0	22·7	11·8					44·7
TED 48	30	975	194	11·5	10·4		1·4	14·4	41·1		5·8	6·7	X	8·6
TED 49	30	1010	147	6·5	5·4		0·9	14·3	38·5		3·6	4·5	X	26·3
TED 45	30	1075	117	3·7	0·9		0·9	15·0	32·0			2·3	X	45·1
APD-664	32	925	145	X					X			X		tr
APD-663	32	1000	173	21·4			1·0	16·8	34·4		17·3	3·9	X	5·2
APD-686	32	1050	79	11·0			1·4	17·6	32·6		5·3	1·0		31·1
APD-680	32	1100	29	5·9			0·9	16·4	27·1					49·7

X, phase is present but modal abundance could not be determined; tr, trace amounts; blank entry, phase is absent. Mineral abbreviations after Kretz (1983).

between 2 and 8 days (Table 2). Temperatures were measured and controlled with W_{74}–Re_{26}/W_{95}–Re_5 thermocouples relative to electronic ice points (0°C) feeding Eurotherm 808 temperature controllers. Temperature stability during all runs was better than ±5°C. The small size of the capsules that were used resulted in the entire sample volume being within 2 mm of the thermocouple. Samples were pressurized at room temperature to about 2 kbar below target pressure, then heated to target temperature and (owing to thermal expansion) the pressure was finally released to target pressure (hot, piston out). The pressures reported are nominal (Heise gauge oil pressures multiplied by ratio of ram-to-piston areas) and were manually maintained within ±0·2 kbar of the target pressure. Oxygen fugacity was not buffered during the experiments, but the graphite-based cell assemblies that are used in the UGA piston-cylinders restrict $\log f\mathrm{O}_2$ in the samples to the interval QFM to QFM−2 (where QFM is the quartz–fayalite–magnetite buffer) (Patiño Douce & Beard, 1994, 1995, 1996; Patiño Douce, 1996). The stabilities and compositions of ferromagnesian phases are not significantly affected by $f\mathrm{O}_2$ variations within this range.

Analytical procedures

Capsules were retrieved from the high-pressure cells by dissolving the NaCl in water. They were inspected under the microscope for tears. Capsules with tears in them were discarded and the experiment was re-run. Phase compositions were determined by electron beam analysis, using the JEOL JXA 8600 electron probe at the University of Georgia, with an accelerating voltage of 15 kV and sample current of 5 nA. To minimize alkali migration, and also to insure accurate targeting, glass analyses were performed in scanning mode at 50 000× magnification, with a focused beam rastered over an area of approximately 4 μm × 4 μm. All other phases were also analyzed in scanning mode but with magnifications typically >100 000×. Na and K were counted first, and Na was counted for 10 s. All other elements were counted for 40 s. Na count rates were corrected as described by Patiño Douce & Harris (1998). In that and other previous studies (e.g. Patiño Douce & Beard, 1995; Patiño Douce, 1996), decay of K count rates was not detected, so that no attempt was made to correct measured K-contents in this study either. Water contents of the experimental glasses were estimated by mass balance (see below).

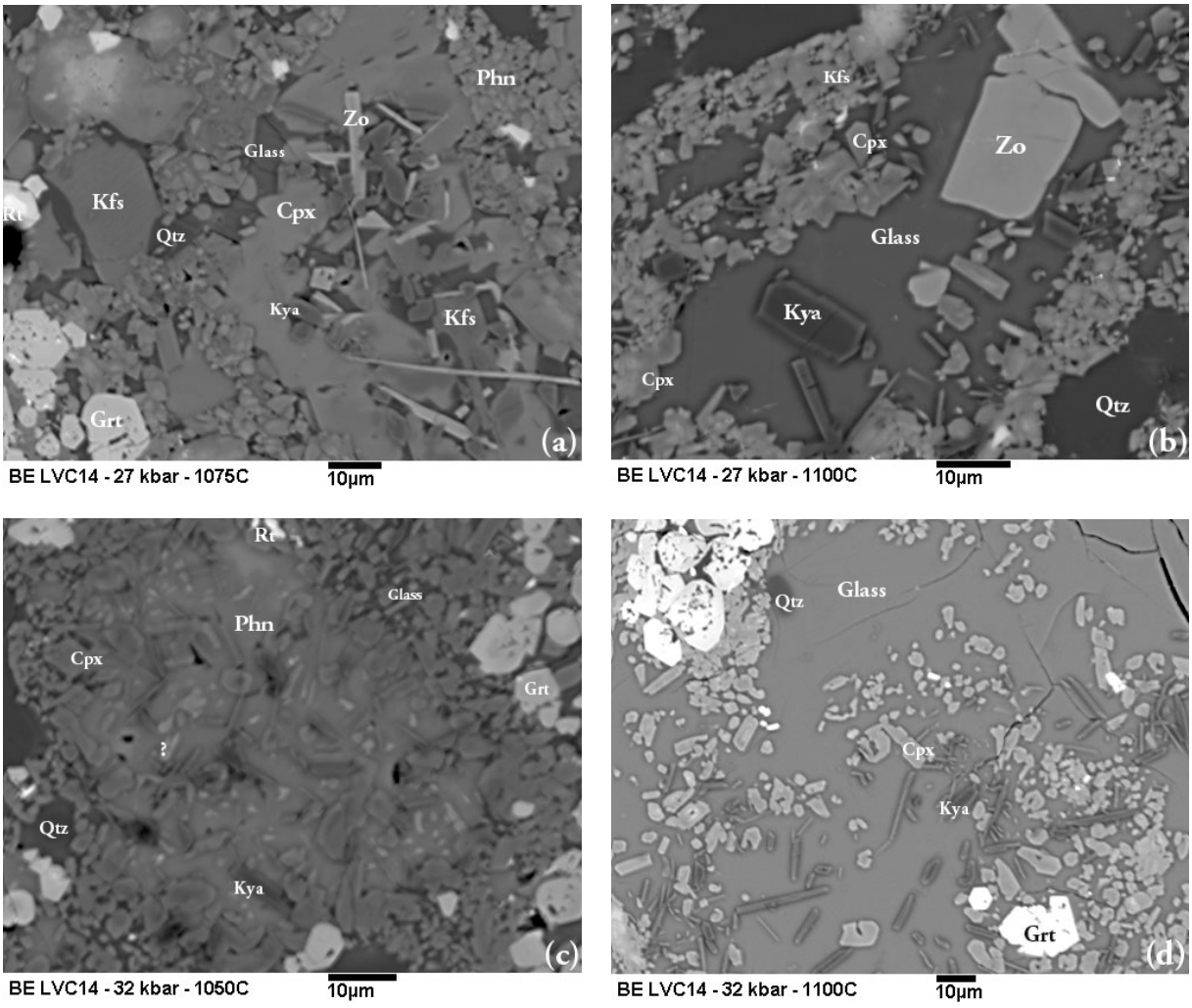

Fig. 2. Back-scattered electron images of selected run products: (a) 27 kbar, 1075°C; (b) 27 kbar, 1100°C; (c) 32 kbar, 1050°C; (d) 32 kbar, 1100°C.

Modal abundances in the experimental products (Table 2) were calculated by a combination of mass balance and partial estimates of modal abundances obtained from back-scattered electron (BSE) images [the method has been described more fully by Patiño Douce & Johnston (1991)]. The oxides used to carry out mass balance were: K_2O, Al_2O_3, SiO_2, MgO, CaO and FeO*. Estimates of modal abundances of melt and total mafic phases, obtained by point-counting BSE images, were included as additional linear equations in the least squares minimization routine, and were given the same weight as the chemical mass-balance equations. This yields a total of eight linear equations, which were solved for the abundances of all phases except rutile (which is always present in trace amounts). Analytical errors and the presence of zoned feldspars (see below) generate uncertainties in the calculated modes of at least ±2 wt % absolute (Patiño Douce, 1995).

DESCRIPTION OF RUN PRODUCTS

The experimental work focused on the pressure range 21–32 kbar, with a few additional experiments run at 15 and 18 kbar. Experimental conditions, phase assemblages and modal compositions of the run products are given in Table 2 and BSE images of selected run products are presented in Fig. 2. Of the two hydrous minerals present in the starting material, only biotite persisted in two supersolidus experiments (at 15 kbar). Amphibole was not observed in any supersolidus experiment. Garnet, clinopyroxene, kyanite, zoisite and phengite crystallized entirely during the experiments, as none of these phases was present in the starting material.

Quartz (or coesite) is present in almost all experiments, as globular or interstitial crystals whose abundance, almost always lower than that in the starting material, decreases with rising temperature. It is only absent from the highest temperature experiment at 21 kbar (1060°C).

Table 3: Feldspar composition (wt %)

P (kbar)	*T* (°C)	SiO_2	Al_2O_3	FeO*	CaO	Na_2O	K_2O	Total
Alkali feldspar								
15	950	66·39	18·98	0·19	0·17	3·17	11·36	100·25
21	940	65·97	19·34	0·15	0·47	4·05	9·88	99·84
21	960	65·21	19·60	0·13	0·99	4·88	8·95	99·76
21	975	66·13	19·45	0·16	0·65	4·29	8·78	99·45
21	1025	66·24	19·61	0·17	0·97	5·73	7·64	100·36
21	1060	64·02	21·45	0·14	2·94	6·18	4·74	99·45
27	1025	64·67	19·44	0·24	0·24	1·58	13·10	99·27
27	1075	64·54	19·94	0·17	0·37	2·82	11·97	99·81
27	1100	64·48	20·04	0·08	1·04	3·37	10·69	99·69
27	1125	65·17	19·91	0·05	1·67	6·10	7·07	99·97
30	975	64·23	19·18	0·16	0·15	1·15	14·50	99·37
30	1010	64·56	19·17	0·14	0·09	1·16	14·13	99·25
30	1075	64·68	19·25	0·12	0·11	1·73	13·54	99·43
Plagioclase								
15	950	57·74	27·28	0·30	8·71	5·99	0·30	100·31
27	1150	54·11	28·60	0·02	11·40	4·81	0·21	99·15

Values are averages of five to seven individual analyses of rims of different grains. Relative analytical uncertainties (±2 S.D. of the average values) are: SiO_2, 2%; Al_2O_3, 1%; FeO*, 25%; CaO, 20% (Kfs) or 2% (Plg); Na_2O, 6%; K_2O, 3% (Kfs) or 25% (Plg).
*Total Fe as FeO.

The SiO_2 phase in some of the 30 and 32 kbar experiments is likely to be coesite, but this was not confirmed as the run products were not subjected to X-ray diffraction analyses.

Kyanite occurs in euhedral tabular and acicular crystals (Fig. 2a–d) in all run products at 21–32 kbar, except at 21 kbar, 1060°C. Its modal abundance is greatest at 21 kbar (up to 6 wt %) and decreases at higher pressures (~1 wt %), in concert with the appearance of zoisite and phengite (Table 2).

Feldspars are present in all run products at pressures of 30 kbar and lower, but not at 32 kbar (Tables 2 and 3). They occur both as euhedral homogeneous crystals (Fig. 2a and b) and as zoned crystals with relic cores mantled by euhedral neoformed rims (Fig. 2a). With the exception of alkali feldspar at 30 kbar, euhedral crystals and rims are compositionally distinct from feldspars in the starting material. Plagioclase is present only at 15 kbar, 950°C, where it coexists with alkali feldspar, and at 27 kbar, 1150°C. Except in this last run, alkali feldspar is always present at 15–30 kbar, but absent at 32 kbar. Its modal abundance decreases with rising temperature and increasing pressure (Table 2). When present at 21–27 kbar, alkali feldspar is always more abundant than in the starting material. It is significantly less abundant at 30 kbar, where it may be largely a relic phase. Alkali feldspar tends to become more Na- and Ca-rich with rising temperature at constant pressure, and less albitic with increasing pressure at constant temperature (Table 3).

Garnet is present in all run products (Tables 2 and 4) as euhedral crystals. No compositional zonation was detected in garnet crystals (Fig. 2a, c and d), probably reflecting that fact that this phase grew entirely during the experiments. Almandine + spessartine contents show little variability within the entire P–T range investigated (Table 4, Fig. 3). From 15 to 27 kbar, garnet also changes little in pyrope and grossular contents. At higher pressures, the grossular content increases noticeably, at the expense of pyrope.

Clinopyroxene is also present in all run products (Tables 2 and 5), generally as subhedral to euhedral unzoned crystals (Fig. 2a–d). Its composition varies regularly with pressure and temperature. There is a clear trend towards higher jadeite contents with increasing pressure but jadeite contents decrease with rising temperature at constant pressure (Figs 4 and 5a and b, Table 5). Jadeite contents in cpx vary antithetically with albite contents in alkali feldspar, reflecting the positive dP/dT slope of the breakdown reaction of albite to jadeite + quartz. Following the classification of Morimoto (1988), experimentally produced clinopyroxene is augite at 15 kbar and omphacite at all higher pressures, except at 27 kbar, 1025°C, where it is jadeite. In addition to these major compositional trends, clinopyroxene shows an excess of $^{[6]}$Al relative to $^{[6]}$Al that is accounted for by the jadeite ($NaAlSi_2O_6$) and Ca-Tschermak's ($CaAlAlSiO_6$) components. The content of 'excess' $^{[6]}$Al is linearly correlated to the amount of vacancies in clinopyroxene (Fig. 5c), clustering close to a line with slope $\frac{1}{2}$. This correlation is consistent with the incorporation of Ca-eskolaite component in clinopyroxene ($Ca_{0.5}\square_{0.5}AlSiO_6$), which generally increases with increasing pressure (Fig. 5d). Clinopyroxene in the 27 kbar, 1025°C experiment is anomalously rich in Al, Na and Ca-eskolaite, for unknown reasons. Ca-eskolaite contents in all other experimental products are generally similar to those reported by Hermann (2002) at comparable experimental conditions.

Micas are present at 15 and 27–32 kbar (Tables 2 and 6). In supersolidus runs, biotite is present only at 15 kbar. Phengite crystallized at 27–32 kbar and is particularly abundant at 32 kbar (Fig. 2a and c). It contains up to 3·3 Si atoms p.f.u, 4–5 wt % FeO + MgO and 1–2 wt % TiO_2. Measured alkali contents (Table 6) may be somewhat low owing to the small size of phengite crystals in some of the run products.

Zoisite crystallized at 27–32 kbar (Fig. 2a and b) and at temperatures of up to 1100°C (at 27 kbar). Compositions

Table 4: Garnet compositions (wt %)

P (kbar)	*T* (°C)	SiO_2	Al_2O_3	TiO_2	FeO*	MgO	MnO	CaO	Na_2O	Total
15	950	39·19	20·44	1·19	24·12	6·31	0·93	7·66	0·10	99·94
21	940	38·89	21·00	0·98	22·39	6·74	0·59	8·70	0·14	99·42
21	960	38·80	20·85	1·22	21·41	8·05	0·69	8·26	0·15	99·43
21	975	39·22	20·88	1·21	22·17	7·70	0·71	8·10	0·12	12·59
21	1025	38·78	20·62	1·27	22·51	7·43	0·59	7·64	0·22	99·05
21	1060	39·18	21·00	1·50	22·24	9·26	0·51	6·56	0·14	100·37
27	1025	37·91	21·61	0·67	26·75	5·61	0·65	6·71	n.d.	99·89
27	1075	38·44	21·41	1·22	23·52	8·39	0·72	5·88	n.d.	99·57
27	1100	37·93	21·56	1·64	23·57	9·23	0·31	5·66	n.d.	99·92
27	1125	39·09	21·35	1·44	21·53	9·83	0·52	5·97	n.d.	99·72
27	1150	38·39	21·58	1·66	20·88	9·49	0·58	7·20	n.d.	99·77
30	975	38·55	21·12	0·52	24·21	3·33	0·80	10·83	0·18	99·54
30	1010	38·08	21·00	0·98	24·65	3·50	0·63	10·16	0·26	99·25
30	1075	39·28	20·79	1·00	22·62	7·80	0·56	6·81	0·36	99·23
32	1000	38·25	20·53	0·57	24·33	2·19	0·74	12·79	0·16	99·56
32	1050	38·64	22·15	0·80	24·23	3·59	0·63	10·05	n.d.	100·09
32	1100	37·75	20·55	0·99	24·51	4·52	0·40	11·04	n.d.	99·76

Values are averages of four to six individual analyses of different grains. Relative analytical uncertainties (±2 S.D. of the average values) are: SiO_2, 2%; Al_2O_3, 2%; TiO_2, 30%; FeO*, 3%; MgO, 5%; MnO, 30%; CaO, 4%; Na_2O, 35%.
*Total Fe as FeO.

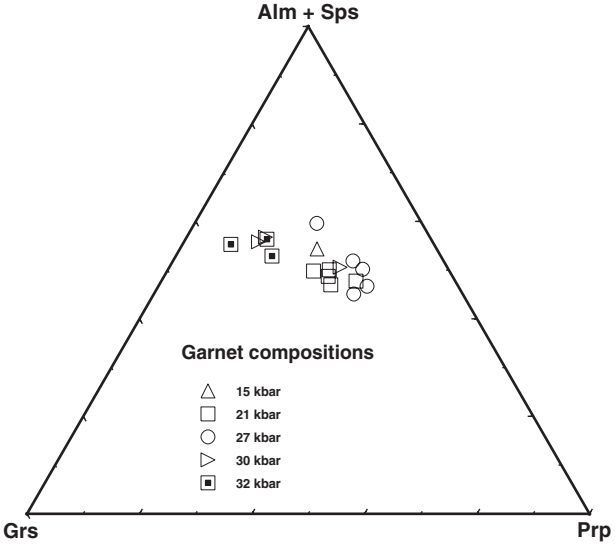

Fig. 3. Molar garnet compositions, recalculated from data in Table 4.

are in every case near end-member zoisite, with negligible Fe^{3+}-contents (Table 7). This may be to some extent a consequence of the strongly reducing conditions (up to ~2 log units below QFM; see above) of the piston-cylinder cell assembly. Whether the phase in the experimental products is zoisite or clinozoisite remains undetermined. It will be called zoisite in this paper, as a generic name.

Rutile is present in all experimental run products in trace amounts, occurring as small crystals, sometimes included in garnet or clinopyroxene (Fig. 2a). No other Fe–Ti oxide phases were found.

Glass (quenched melt) is present in all experiments except at 18 kbar, 900°C and 27 kbar, 1000°C (Fig. 2). Glass compositions and modal abundances (Tables 2 and 8) could be determined in all melt-bearing experiments except at 15 kbar, 900°C and 32 kbar, 925°C, where it is present in trace amounts. Glass compositions are homogeneous throughout each experimental charge in which it could be analyzed. The compositions in Table 8 are recalculated to 100 wt % H_2O-free. Original microprobe totals and H_2O-contents estimated by mass balance (assuming 2·5 wt % H_2O in zoisite and 3·5 wt % H_2O in phengite) are also included in Table 8. With a few exceptions, there is good agreement between these estimated H_2O-contents and the difference between microprobe totals and 100%. The discrepancies arise from uncertainties in the glass compositions, and the resulting microprobe totals, compounded with uncertainties in the calculation of modal compositions. Water contents estimated by mass balance are probably a better approximation to melt H_2O-contents than differences from 100%.

Table 5: Clinopyroxene composition (wt %)

P (kbar)	*T* (°C)	SiO_2	Al_2O_3	TiO_2	FeO*	MgO	MnO	CaO	Na_2O	K_2O	Total
15	950	53·21	4·74	0·48	11·72	12·84	0·23	15·40	1·11	0·10	99·82
21	940	52·81	11·06	0·75	6·00	9·56	0·15	14·38	4·06	0·42	99·19
21	960	52·87	9·45	0·70	6·06	11·53	0·18	15·65	3·43	0·11	99·98
21	975	53·98	9·99	0·71	5·92	11·21	0·11	15·01	3·68	0·10	100·71
21	1025	53·06	8·67	0·66	7·22	10·94	0·20	15·87	3·39	0·05	100·07
21	1060	52·22	10·72	0·90	3·89	11·38	0·19	18·04	3·00	0·08	100·41
27	1025	57·07	25·13	0·09	1·32	0·30	0·09	6·07	9·53	0·06	99·66
27	1075	53·64	18·65	0·76	3·12	4·49	0·11	10·96	7·21	0·06	98·98
27	1100	52·51	19·10	1·31	3·62	4·15	0·15	12·10	6·98	0·03	99·95
27	1125	52·15	18·42	1·16	3·96	4·91	0·13	12·97	5·91	0·12	99·73
27	1150	51·61	17·06	1·11	4·71	6·43	0·15	13·51	5·22	0·05	99·85
30	975	55·70	17·68	0·37	4·89	4·07	0·13	8·85	7·76	0·11	99·54
30	1010	55·65	19·21	0·40	4·13	3·62	0·05	9·03	7·64	0·16	99·88
30	1075	54·72	14·56	0·71	5·98	6·21	0·12	10·46	6·44	0·09	99·29
32	1000	55·88	21·01	0·23	3·58	2·88	0·00	7·94	8·45	0·19	100·16
32	1050	54·49	19·92	0·48	4·19	4·13	0·00	8·84	8·16	0·05	100·26
32	1100	53·63	19·60	0·61	4·93	3·05	0·22	10·50	7·65	0·09	100·28

Values are averages of seven to ten individual analyses of different grains. Relative analytical uncertainties (±2 S.D. of the average values) are: SiO_2, 2%; Al_2O_3, 4%; TiO_2, 30%; FeO*, 5%; MgO, 5%; MnO, 30%; CaO, 4%; Na_2O, 5%; K_2O, 50%. *Total Fe as FeO.

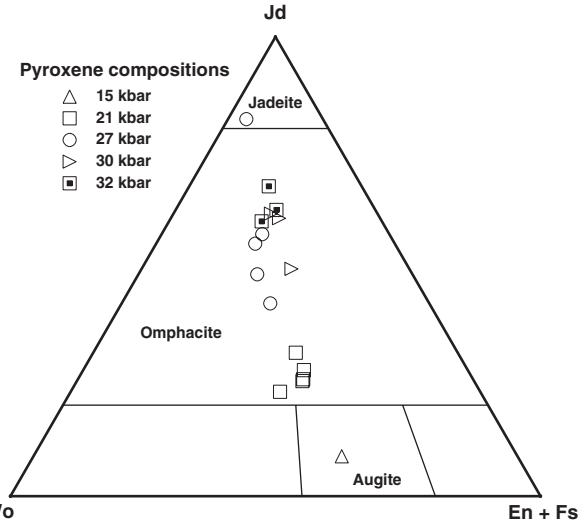

Fig. 4. Molar clinopyroxene compositions, recalculated from data in Table 5. Jadeite, omphacite and augite fields after Morimoto (1988).

APPROACH TO EQUILIBRIUM

Equilibrium cannot be strictly demonstrated in the absence of reversals. Patiño Douce (1995), Patiño Douce & Beard (1995) and Patiño Douce & Harris (1998) used a limited number of reversals to show that melt-present experiments performed under vapor-absent conditions generally approach equilibrium. Virtually all of the phases found in the melt-bearing experiments discussed here are neoformed (i.e. they were not present in the starting material) and reasonably euhedral (Fig. 2), and they vary regularly in composition with changes in *P* and *T*. The compositions of melts and solid phases are constant throughout each experimental charge. These observations are consistent with a good approach to equilibrium in those experiments in which a melt phase was present. Unmolten experiments, on the other hand, clearly did not achieve equilibrium, as the minerals that are present in them are unchanged from those in the starting material. There obviously are strong kinetic impediments to reaction in the absence of a fluid phase, which keep hydrous minerals from reacting out until the vapor-absent solidus has been significantly overstepped. In vapor-absent experiments such as these, performed with starting materials equilibrated in nature at pressures far removed from the experimental conditions, there is thus an unavoidable gap between subsolidus experiments that never attain equilibrium and experiments that equilibrate a finite distance above the solidus. This gap makes it impossible to determine the exact location of the vapor-absent solidus. It is nevertheless possible to extract very valuable phase equilibrium information from super-solidus experiments that have approached equilibrium, as discussed in the following section.

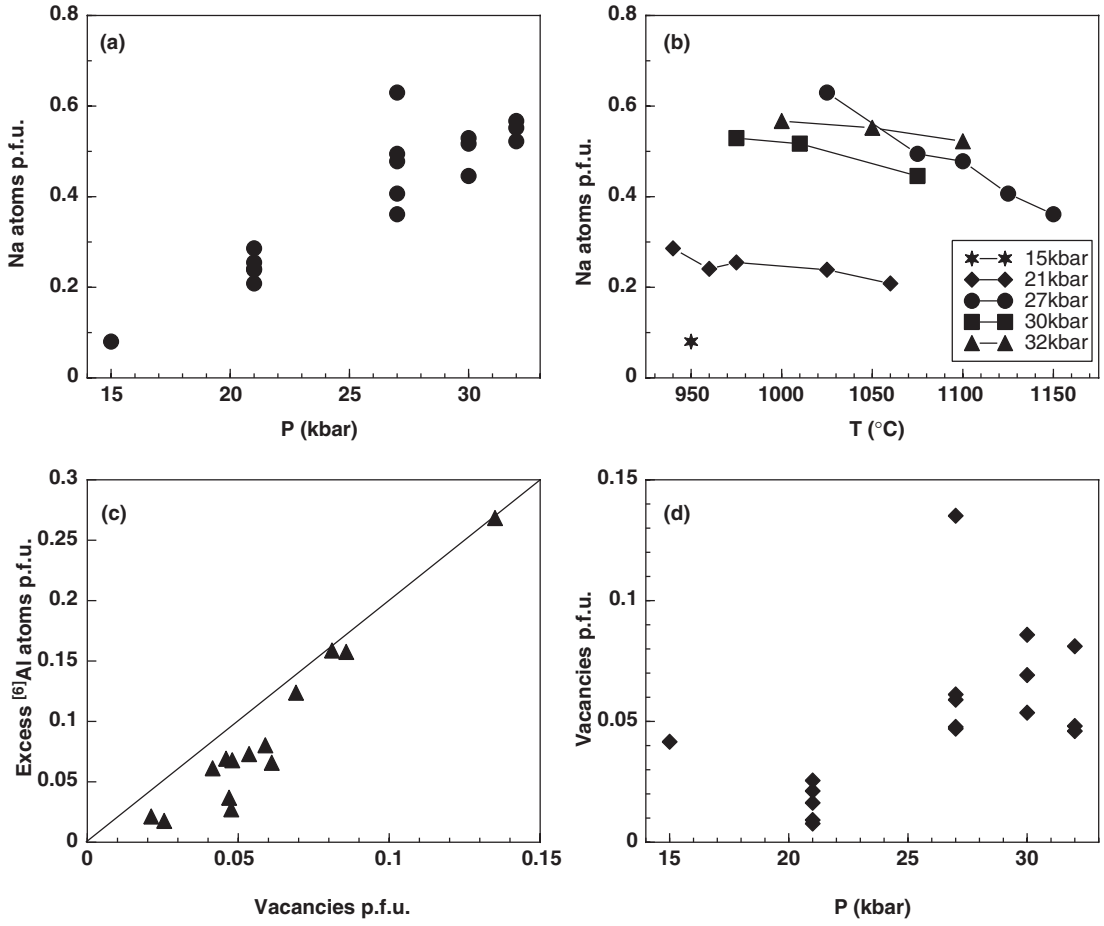

Fig. 5. Atomic clinopyroxene compositions, recalculated from data in Table 5 on a 6 oxygen basis. (a) and (b) Na-contents (=jadeite) as a function of pressure and temperature; (c) correlation between excess octahedral Al (i.e. octahedral Al not accounted for by jadeite nor Ca-Tschermak's components) and vacancies. The line with a slope of 2 corresponds to the Ca-eskolaite component; (d) vacancy contents (proxying for Ca-eskolaite) as a function of pressure.

Table 6: Mica compositions (wt %)

P (kbar)	*T* (°C)	SiO_2	Al_2O_3	TiO_2	FeO*	MgO	MnO	CaO	Na_2O	K_2O	F	Total	Tot − F eq.[1]
Phengite													
27	1025	48·23	32·00	0·24	2·47	0·97	0·00	0·07	0·17	9·44	0·00	93·58	93·58
27	1075	48·52	33·44	0·23	1·68	0·69	0·13	0·04	0·53	9·30	0·18	94·71	94·63
30	975	50·75	30·40	1·25	2·45	1·93	0·01	0·10	0·35	9·27	0·25	96·76	96·65
30	1010	48·83	29·87	2·24	2·09	2·04	0·06	0·05	0·30	10·50	0·23	96·21	96·11
32	1000	50·68	29·81	1·77	2·23	2·08	0·02	0·16	0·33	10·42	0·22	97·72	97·63
32	1050	48·94	29·54	1·42	2·31	2·71	0·26	0·09	0·14	9·33	0·58	95·32	95·08
Biotite													
15	950	40·14	15·96	6·24	11·02	14·52	0·08	0·07	0·51	9·08	0·82	98·41	98·07

Values are averages of six to ten individual analyses of different grains. Relative analytical uncertainties (±2 S.D. of the average values) are: SiO_2, 2%; Al_2O_3, 2%; TiO_2, 10%; FeO*, 8%; MgO, 10%; MnO, 50%; CaO, 30%; Na_2O, 10%; K_2O, 5%; F, 25%.
*Total Fe as FeO.
[1]Total minus fluorine oxygen-equivalent.

Table 7: Zoisite composition (wt %)

P (kbar)	*T* (°C)	SiO_2	Al_2O_3	TiO_2	FeO*	MgO	MnO	CaO	Na_2O	K_2O	Total
27	1025	39·26	32·81	0·02	0·79	0·01	0·02	24·63	0·09	0·14	97·75
27	1075	39·95	32·10	0·03	0·71	0·00	0·22	23·30	0·08	0·11	96·50
27	1100	39·39	32·71	0·22	0·84	0·13	0·04	23·67	0·07	0·08	97·15
30	975	40·58	33·83	0·06	0·44	0·00	0·00	23·11	0·14	0·28	98·44
30	1010	40·43	32·74	0·06	0·60	0·01	0·06	23·21	0·15	0·29	97·55
30	1075	40·19	32·99	0·09	1·26	0·06	0·14	22·70	0·16	0·35	97·94
32	1000	39·69	33·50	0·01	0·29	0·01	0·00	23·71	0·09	0·14	97·44
32	1050	39·58	33·24	0·01	0·37	0·02	0·00	23·62	0·12	0·15	97·11

Values are averages of four to six individual analyses of different grains. Relative analytical uncertainties (±2 S.D. of the average values) are: SiO_2, 2%; Al_2O_3, 2%; TiO_2, 50%; FeO*, 12%; MgO, 60%; MnO, 50%; CaO, 1%; Na_2O, 30%; K_2O, 30%.
*Total Fe as FeO.

Table 8: Glass compositions (wt %)

P (kbar)	*T* (°C)	SiO_2	Al_2O_3	TiO_2	FeO*	MgO	MnO	CaO	Na_2O	K_2O	F	H_2O[1]	Total[2]
15	950	73·17	15·02	0·30	0·89	0·33	0·02	1·11	4·67	4·50	0·00	5·1	96·87
21	940	73·00	15·74	0·21	0·50	0·27	0·03	0·94	5·51	3·81	0·09	9·8	96·61
21	960	72·67	15·60	0·30	0·83	0·27	0·00	1·17	5·25	3·91	0·20	8·1	95·66
21	975	72·63	15·85	0·21	0·70	0·23	0·10	1·12	5·20	3·95	0·07	6·3	95·70
21	1025	72·89	15·32	0·38	1·15	0·22	0·01	0·89	4·99	4·14	0·07	3·1	95·92
21	1060	71·25	16·14	0·49	0·69	0·39	0·06	1·52	4·05	5·41	0·16	1·8	95·54
27	1025	73·41	15·55	0·11	0·42	0·04	0·03	0·79	2·77	6·88	0·03	8·5	92·36
27	1075	74·86	16·44	0·10	0·42	0·03	0·02	0·97	3·02	4·14	0·10	3·8	92·10
27	1100	73·80	16·57	0·29	0·78	0·11	0·03	1·09	3·04	4·30	0·16	3·5	95·14
27	1125	71·48	16·32	0·52	0·78	0·24	0·03	1·55	3·85	5·23	0·14	2·5	96·42
27	1150	70·64	16·54	0·59	0·97	0·26	0·01	1·76	3·91	5·32	0·21	2·2	98·18
30	975	75·48	16·62	0·17	0·52	0·10	0·02	0·98	2·10	4·00	0·19	7·3	93·43
30	1010	73·51	15·44	0·18	0·69	0·07	0·00	0·78	3·11	6·22	0·07	2·9	93·68
30	1075	72·16	16·05	0·37	0·65	0·12	0·03	0·88	3·60	6·13	0·27	2·1	94·35
32	1000	70·79	16·37	0·09	0·54	0·11	0·05	1·56	4·18	6·31	0·13	5·8	94·71
32	1050	73·30	16·08	0·21	0·59	0·08	0·07	0·93	3·92	4·83	0·14	2·5	93·59
32	1100	70·10	16·43	0·51	1·28	0·29	0·04	2·01	4·20	5·14	0·08	2·0	98·01

Values are averages of five to ten individual glass pools. Relative analytical uncertainties (±2 S.D. of the average values) are: SiO_2, 2%; Al_2O_3, 3%; TiO_2, 15%; FeO*, 10%; MgO, 20%; MnO, 50%; CaO, 5%; Na_2O, 10%; K_2O, 5%; F, 40%.
*Total Fe as FeO.
[1]Glass H_2O-contents calculated from modal compositions (Table 2), assuming 1 wt % bulk H_2O-content (see text).
[2]Original probe totals. Glass compositions are given recalculated to 100 wt % water-free.

PHASE RELATIONS

The phase assemblages produced in the tonalite melting experiments are summarized in Fig. 6. Neither biotite nor amphibole is present in experiments that contain even traces of melt at $P \geq 21$ kbar. The only hydrous phases present in such experiments, besides melt, are phengite and zoisite (Fig. 6, Table 2). These observations suggest that when some amount of fluid becomes available in the experimental charges (by breakdown of one or both hydrous phases in the starting material, and possibly after overstepping of the vapor-absent solidus), other hydrous phases that are stable at the experimental

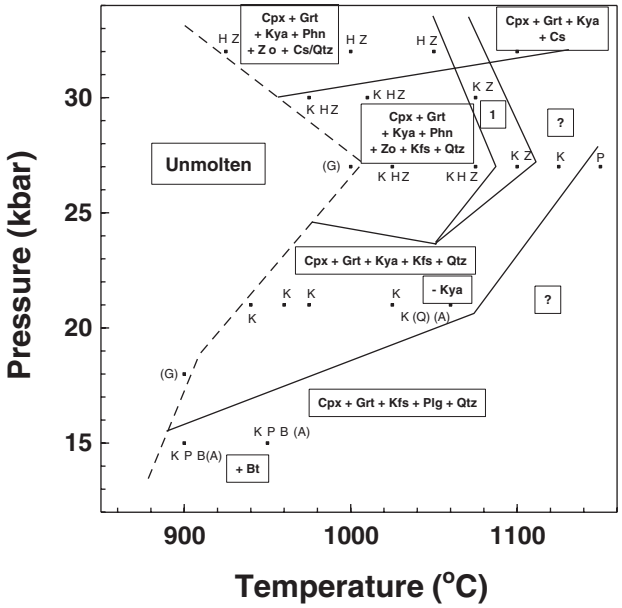

Fig. 6. Phase assemblages in experimental run products. All experiments contain garnet and clinopyroxene. All also contain quartz (or coesite) and aluminosilicate, except those labeled (Q) and (A), respectively. In addition, experiments may contain phengite, H; zoisite, Z; K-feldspar, K; plagioclase, P; and biotite, B. Subsolidus experiments are labeled (G). Field 1 contains the assemblage Cpx + Grt + Ky + Zo + Kfs + Qtz. The dashed line separates melt-bearing from unmolten experiments but is not the vapor-absent solidus (see text for discussion).

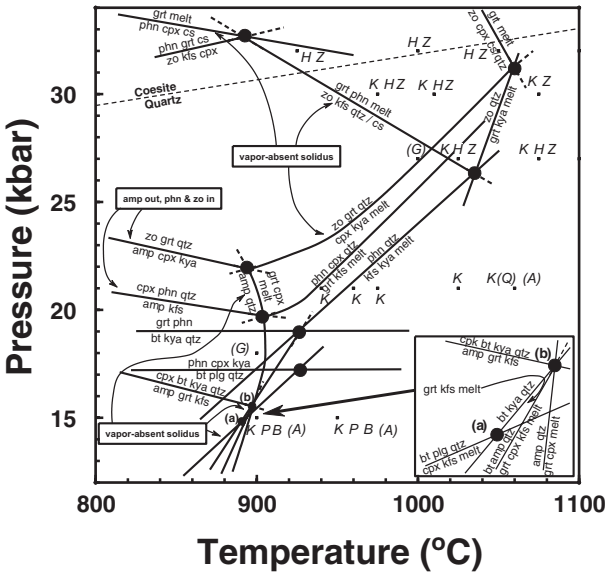

Fig. 7. Phase diagram for vapor-absent melting of tonalite in the deep crust and upper mantle. The diagram shows univariant equilibria in the system K_2O–Al_2O_3–MgO–CaO–SiO_2–H_2O, calibrated with experimental data summarized in Fig. 6. In natural assemblages, the equilibria will have higher variance and will display considerable overlap. The subsolidus P–T interval over which amphibole reacts out to phengite + zoisite-bearing assemblages and the vapor-absent solidus at $P > 20$ kbar are located only approximately (see text). Inset shows detail of biotite and amphibole dehydration-melting reactions at pressures in the neighborhood of 15 kbar. The quartz–coesite phase boundary is shown for reference; identity of the SiO_2 phase in the experimental products was not determined.

conditions crystallize rapidly, even if the end-product of this reaction contains relatively little hydrous melt (e.g. Table 2). I have combined the near-solidus results with a geometrical analysis of phase relations in order to construct a model for the UHP vapor-absent melting behavior of tonalitic rocks. Because the experimental results suggest that phengite and zoisite are the phases that are likely to control dehydration-melting of tonalites at UHP conditions, the model also seeks to explain subsolidus crystallization of these phases from breakdown of the low-pressure hydrous phase assemblage present in tonalites (biotite + hornblende).

The resulting phase diagram is shown in Fig. 7. The phase boundaries shown in this diagram are based on a geometrical analysis of the system K_2O–Al_2O_3–MgO–CaO–SiO_2–H_2O, and of course translate into higher variance fields in natural systems. Their P–T locations are constrained by results from the experiments presented here (Fig. 6) as well as by those of previous workers, as discussed below. I must emphasize that the diagram in Fig. 7 is not intended to be an exhaustive analysis of phase relations in the K_2O–Al_2O_3–MgO–CaO–SiO_2–H_2O system. In particular, it is strictly applicable only to tonalite bulk compositions and only in the absence of a free aqueous fluid phase. More general analyses of UHP phase relations in the system K_2O–Al_2O_3–MgO–CaO–SiO_2–H_2O have been given by Hermann & Green (2001) and Hermann (2002). Note that there are some important differences between the phase relations proposed in those studies and the ones presented here, especially with respect to the stability of ferromagnesian phases. Thus, orthopyroxene and talc were among the phases observed experimentally by Hermann & Green (2001) and Hermann (2002), but neither of them was present in my experiments. This difference arises primarily from the strong effect of Fe/Mg ratio on the stabilities of pyroxenes, talc and garnet, and also reflects, in the case of talc, the higher H_2O activity in Hermann & Green's H_2O-saturated experiments compared with my fluid-absent experiments.

Biotite and amphibole dehydration-melting in the deepest continental crust ($P \sim 15$ kbar)

Several biotite and amphibole dehydration-melting reactions converge at $P \sim 15$ kbar (Fig. 7, inset). In kyanite-free assemblages such as tonalites, vapor-absent melting at this pressure begins with the reaction [mineral abbreviations after Kretz (1983)]:

$$\mathrm{Bt} + \mathrm{Amp} + \mathrm{Plg} + \mathrm{Qtz} \rightarrow \mathrm{Cpx} + \mathrm{Grt} + \mathrm{Kfs} + \mathrm{Melt}. \quad (1)$$

This reaction is supported by the significant abundance of garnet and clinopyroxene in the 15 kbar, 950°C melting experiment (Table 2), as well as by the increased abundance of K-feldspar in this experiment relative to the starting composition. Reaction (1) results from the overlap of the multivariant fields associated with the following two reactions, shown in Fig. 7 (inset):

$$\text{Bt} + \text{Plg} + \text{Qtz} \rightarrow \text{Cpx} + \text{Kfs} + \text{Melt} \quad (2)$$

and

$$\text{Bt} + \text{Amp} + \text{Qtz} \rightarrow \text{Grt} + \text{Cpx} + \text{Kfs} + \text{Melt}. \quad (3)$$

With decreasing pressure, reaction (2) defines the vapor-absent solidus (Fig. 7, inset). Note that this reaction is different from even lower-pressure, orthopyroxene-forming biotite dehydration-melting reactions (e.g. Vielzeuf & Montel, 1994; Patiño Douce & Beard, 1995; Vielzeuf & Schmidt, 2001). Direct evidence supporting reaction (2) is given by the formation of clinopyroxene as a peritectic phase in the 15 kbar melting experiments on the biotite + plagioclase + quartz assemblage studied by Patiño Douce & Beard (1995). Transition between opx-forming and cpx-forming biotite melting reactions takes place at $P \sim 12$–13 kbar (Patiño Douce & Beard, 1995) and is not addressed in this study.

At pressures higher than 15 kbar, the amphibole dehydration melting reaction

$$\text{Amp} + \text{Qtz} \rightarrow \text{Cpx} + \text{Grt} + \text{Melt} \quad (4)$$

replaces reaction (1) on the tonalite vapor-absent solidus (Fig. 7, inset). This reaction, however, was not observed in any of the experiments reported here, probably because it is kinetically inhibited in vapor-absent experimental charges. It is located in Fig. 7 after Vielzeuf & Schmidt (2001, fig. 5).

Analysis of the phase relations suggests that the first subsolidus appearance of phengite in tonalites is likely to be a result of the following water-conserving reaction:

$$\text{Bt} + \text{Plg} + \text{Qtz} \rightarrow \text{Phn} + \text{Cpx} + \text{Ky} \quad (5)$$

which causes plagioclase to disappear from the subsolidus tonalite assemblage and stabilizes the phengite + quartz dehydration-melting reaction

$$\text{Phn} + \text{Qtz} \rightarrow \text{Kfs} + \text{Ky} + \text{Melt}. \quad (6)$$

The experiments suggest that reaction (5) takes place in the interval 15–21 kbar (Figs 6 and 7). The large modal abundance of kyanite and absence of both micas in the 21 kbar experiments (Table 2) suggest that at the P–T conditions of those experiments, reactions (5) and (6) have both been crossed.

Subsolidus amphibole elimination and high-temperature phengite + zoisite melting in the upper mantle ($P \sim 20$–27 kbar)

The dehydration-melting solidus of amphibole + quartz in basaltic bulk compositions undergoes a strong back-bending at pressures between ~15 and 25 kbar (Wyllie & Wolf, 1993; Vielzeuf & Schmidt, 2001). The negatively sloping segment of the amphibole + quartz vapor-absent solidus, however, may be largely suppressed in tonalites. The reason for this is that amphibole undergoes subsolidus water-conserving terminal reactions in tonalites that are not possible in amphibolites. Three such reactions are shown in Fig. 7. Two of these reactions depend on the availability of K-feldspar as a reactant—a phase that is present in tonalites but not in basaltic amphibolites. The third one requires kyanite as a reactant, which is likely to form in tonalites (but not in amphibolites) by subsolidus breakdown of biotite + plagioclase [reaction (5)].

Amphibole elimination as pressure increases could begin with the following reaction, which would only take place if garnet was formed by some other lower-pressure reaction:

$$\text{Amp} + \text{Grt} + \text{Kfs} \rightarrow \text{Bt} + \text{Cpx} + \text{Ky} + \text{Qtz}. \quad (7)$$

This reaction is followed at successively higher pressures by the phengite-forming reaction

$$\text{Amp} + \text{Kfs} \rightarrow \text{Phn} + \text{Cpx} + \text{Qtz} \quad (8)$$

and by the zoisite-forming reaction

$$\text{Amp} + \text{Cpx} + \text{Ky} \rightarrow \text{Zo} + \text{Grt} + \text{Qtz} \quad (9)$$

neither of which requires garnet as a reactant. The experiments provide evidence for reactions (8) and (9). This evidence rests on the presence of phengite and zoisite, but no amphibole, in low melt fraction experiments at 27 kbar. The topology of the phase relations (see Fig. 7) requires that reaction (9) occurs at higher pressure than reaction (8). In natural multivariant assemblages, however, the two reactions are likely to overlap, leading to a P–T interval over which amphibole is progressively eliminated in favor of the hydrous assemblage zoisite + phengite.

The following two dehydration-melting reactions become stable on the high-pressure side of reactions (8) and (9), respectively:

$$\text{Phn} + \text{Cpx} + \text{Qtz} \rightarrow \text{Grt} + \text{Kfs} + \text{Melt} \quad (10)$$

and

$$\text{Zo} + \text{Grt} + \text{Qtz} \rightarrow \text{Cpx} + \text{Ky} + \text{Melt}. \quad (11)$$

Vapor-absent melting of tonalites at pressures of the order of 25 kbar should thus begin with breakdown of zoisite + garnet + quartz, followed by breakdown of

phengite + clinopyroxene + quartz (with the two reactions almost certainly overlapping in natural multivariant assemblages).

The experimental results are consistent with subsolidus elimination of amphibole from tonalites within the pressure range 20–25 kbar. This conclusion is reached (see Fig. 7) if one assumes that the melt-absent experiment at 27 kbar, 1000°C is on the low-temperature side of reaction (11) and that the experiment at 21 kbar, 940°C, which contains melt but no solid hydrous phases, is on the high-temperature side of reaction (10). Note that even though there is considerable uncertainty in this argument (because these experiments do not constrain the solidus), the near-horizontal slope of the amphibole + quartz solidus at $P \sim 25$ kbar constitutes an effective upper pressure limit for amphibole-controlled dehydration-melting (see Vielzeuf & Schmidt, 2001). Zoisite and/or phengite must define the vapor-absent solidus at higher pressures, as shown by the fact that these are the hydrous phases that coexist with melt in near-solidus experiments at these conditions (see also Skjerlie & Patiño Douce, 2002).

Backbending of the vapor-absent solidus at $P > 27$ kbar

The tonalite melting experiments suggest that there is a strong back-bending of the vapor-absent solidus at pressures between 25 and 30 kbar (Figs 6 and 7). This back-bending was also observed during vapor-absent melting of a zoisite- and phengite-bearing basaltic eclogite by Skjerlie & Patiño Douce (2002), who suggested that it reflects the switch from a phengite-controlled solidus to a zoisite-controlled solidus. Vielzeuf & Schmidt (2001) also proposed a negatively sloping Zo + Cpx vapor-absent solidus for basaltic bulk compositions at $P > 25$ kbar. The situation in tonalites is more complex, as the back-bending appears to be caused not by a switch from a phengite-controlled solidus to a zoisite-controlled solidus, but rather by a switch between two distinct zoisite melting reactions.

Zoisite almost certainly controls the tonalite vapor-absent solidus from the pressure at which amphibole disappears (~20–25 kbar) to at least 32 kbar (see Fig. 7). Within the lower portion of this pressure range, the solidus is defined by the zoisite + garnet + quartz dehydration-melting reaction (11). The experimental constraints, the topology of the phase diagram and the fact that the high-density phase garnet is a reactant all argue in favor of this reaction having a positive dP/dT slope. At pressures of the order of 27–30 kbar, reaction (11) is intersected by the zoisite + K-feldspar + quartz (or coesite) dehydration-melting reaction

$$\mathrm{Zo} + \mathrm{Kfs} + \mathrm{Qtz/Cs} \rightarrow \mathrm{Phn} + \mathrm{Grt} + \mathrm{Melt}. \qquad (12)$$

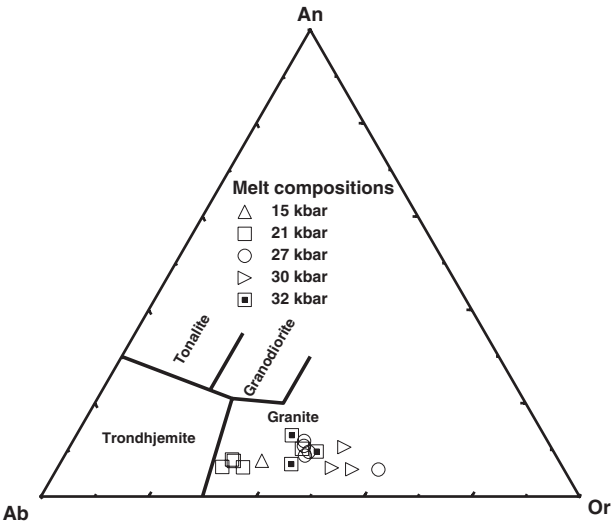

Fig. 8. Normative Ab–An–Or compositions of experimental melts. Classification of silicic melts from Barker (1979).

This reaction may appear unusual, as it includes an anhydrous potassic phase among the reactants and produces peritectic phengite. It is justified by the noticeable increase in the modal abundance of phengite and concomitant decreases in the zoisite and K-feldspar abundances from 30 to 32 kbar (Table 2). These changes in modal abundances together with the observed decrease in the melt-in temperature from 27 to 32 kbar, the topology of phase relations and the fact that garnet is now a product of the peritectic melting reaction are all arguments that support the negative dP/dT slope of reaction (12). A negatively sloping zoisite + clinopyroxene + quartz melting reaction, similar to the one proposed by Vielzeuf & Schmidt (2001) for amphibolites, is also possible in tonalites but must be located at a higher temperature than reaction (12), as shown in Fig. 7. The fact that initial melts at 30–32 kbar are K-rich indicates that the high-pressure tonalite solidus must be defined by a reaction that includes a K-rich phase among the reactants, such as the zoisite + K-feldspar dehydration-melting reaction (12).

MELT AND RESIDUE CHARACTERISTICS

Melt compositions in all the experiments are silica- and alumina-rich ($SiO_2 > 70$ wt %, $Al_2O_3 > 15$ wt %), leucocratic (FeO + MgO + $TiO_2 < 2{\cdot}1$ wt %) and peraluminous (Table 8). All melts are granitic (Fig. 8), with K/Na ratios that vary consistently with pressure. The most sodic melts, approaching trondhjemitic compositions, were produced at 21 kbar, whereas the most potassic melts

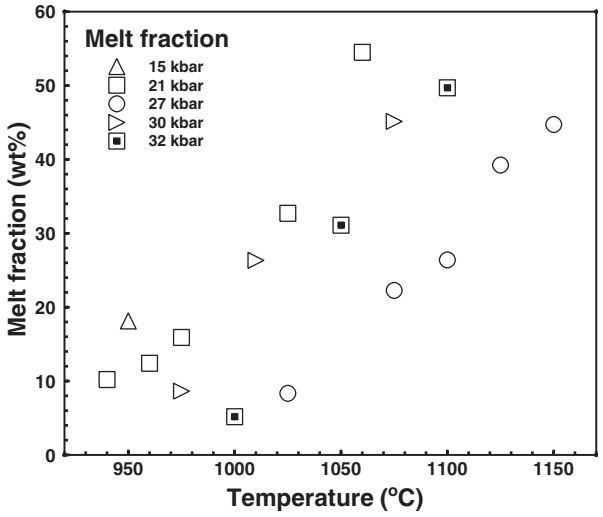

Fig. 9. Calculated melt fractions (wt %) as a function of temperature and pressure.

were, with one exception, those produced at 30 kbar (the exception is the lowest-temperature 27 kbar melt). These variations in K/Na ratio reflect the effects of pressure on clinopyroxene composition (the Na reservoir) and phengite and alkali feldspar stabilities (the K reservoirs). Contents of mafic oxides also vary regularly with pressure and temperature. At constant temperature, melts are most leucocratic at 27 kbar and less so at 21 kbar, but all melts are strictly leucogranitic (Table 8).

Melt fractions at the experimental conditions that were investigated are in almost every case lower than 50 wt % and, at constant temperature, they are lowest at 27 kbar than at higher and lower pressures (Fig. 9). The melt abundance minimum is consistent with back-bending of the vapor-absent solidus at a pressure of the order of 27 kbar and the existence of a maximum in solidus temperature at this pressure (Fig. 7).

The residues formed in experiments at pressures of 21 kbar and greater are quartz eclogites, composed dominantly of garnet + omphacitic clinopyroxene + quartz or coesite (Table 2). Potassium feldspar is also a major phase at pressures of up to approximately 27 kbar, and both phengite and zoisite are fairly abundant in near-solidus runs at 27–32 kbar. Table 9 shows calculated 1 bar densities and alkali and water contents of the residual assemblages. Residues formed at $P > 20$ kbar after extraction of a minimum of 20–30% melt have densities $\geq 3{\cdot}3$ g/cm^3, that are comparable with those of mantle rocks (Fig. 10). It is noteworthy that some of these high-density, melt-depleted residual assemblages contain up to a few tenths of a wt % H_2O (bound in zoisite and phengite) and 4–6 wt % K_2O + Na_2O (bound in phengite, K-feldspar and clinopyroxene).

Table 9: Densities and water and alkali contents of residues

P (kbar)	T (°C)	Density (g/cm^3)	Na_2O (wt %)	K_2O (wt %)	H_2O (wt %)
15	950	3·05	2·7	2·2	0·1
21	940	3·14	2·8	3·2	0·0
21	960	3·19	2·5	3·0	0·0
21	975	3·22	2·4	2·9	0·0
21	1025	3·29	2·6	2·3	0·0
21	1060	3·47	2·5	1·3	0·0
27	1025	3·19	3·4	2·5	0·3
27	1075	3·28	3·2	2·0	0·2
27	1100	3·31	3·4	1·8	0·1
27	1125	3·41	3·2	0·9	0·0
27	1150	3·39	2·0	0·0	0·0
30	975	3·27	3·7	2·3	0·4
30	1010	3·36	4·1	1·6	0·3
30	1075	3·50	3·8	0·3	0·1
32	1000	3·23	3·2	2·0	0·8
32	1050	3·39	3·9	0·6	0·3
32	1100	3·51	4·1	0·0	0·0

Values are calculated from modal compositions in Table 2, recalculated to 100 wt % glass-free, and mineral compositions. H_2O-contents assume difference from 100% in phengite and zoisite analyses is H_2O.

DISCUSSION

There have been few previous experimental studies of UHP melting relations of tonalites. With the exception of the study by Patiño Douce & McCarthy (1998), which was a preliminary and partial presentation of the results discussed here, the other UHP tonalite melting studies have been under conditions of H_2O-saturation (Lambert & Wyllie, 1974; Carroll & Wyllie, 1990; Schmidt, 1993; Schmidt & Thompson, 1996). As expected, the tonalite water-saturated solidus occurs at much lower temperatures (up to ~300°C at 25–30 kbar) than the dehydration-melting solidus [Fig. 11, H_2O-saturated solidus after Lambert & Wyllie (1974) and Schmidt (1993)]. Similarly, the H_2O-saturated solidus of zoisite + quartz/coesite (after Poli & Schmidt, 1995) is located at a temperature 200–250°C lower than the zoisite + K-feldspar + quartz/coesite vapor-absent solidus (Fig. 11).

Significant comparisons can also be made with amphibole + quartz dehydration-melting in basaltic amphibolites [solidus shown in Fig. 11 after Vielzeuf & Schmidt (2001)] and with the phengite + coesite + clinopyroxene vapor-absent solidus in the end-member KCMASH system (Hermann & Green, 2001). The amphibole + quartz solidus becomes nearly vertical at $P \approx 10$ kbar, and then undergoes a strong back-bending, beginning at pressures

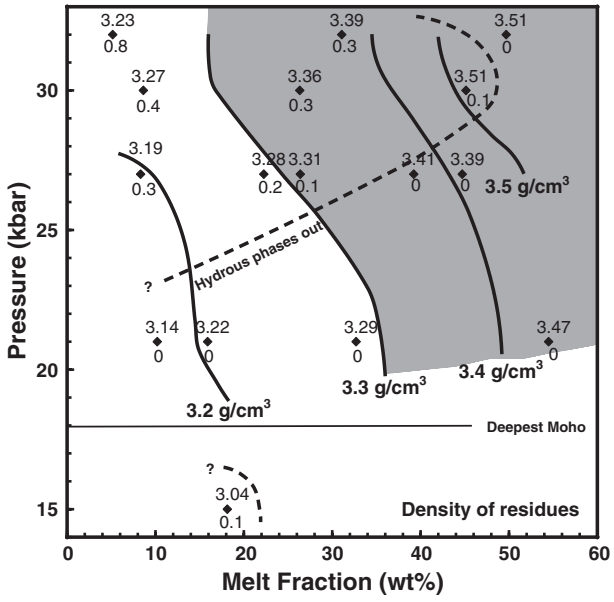

Fig. 10. Calculated densities (numbers above *P–T* points) and H_2O-contents (numbers below *P–T* points) of experimentally generated residues (see Table 9). Continuous-line contours show densities of residues. Dashed contours show approximate conditions at which hydrous phases vanish from the residues. Shaded area shows range of conditions under which residues of partial melting of tonalites have densities comparable with those of mantle rocks and would thus be able to remain entrained in the mantle indefinitely. 'Deepest Moho' shows the approximate pressure at the bottom of the thickest known continental crust (~70 km).

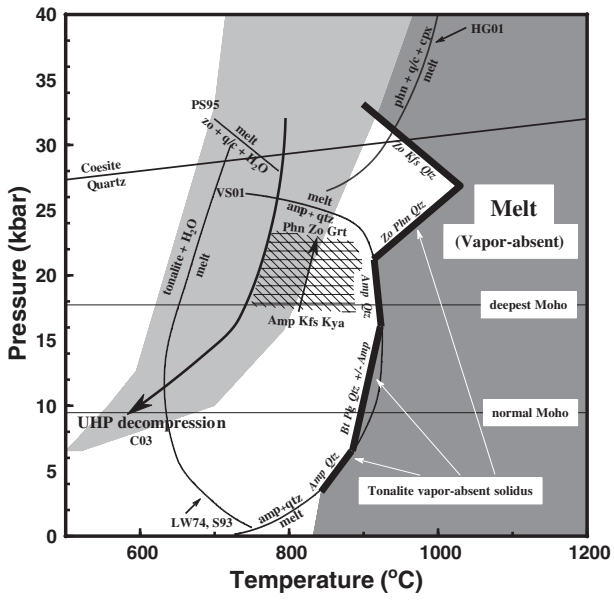

Fig. 11. Phase relations and *P–T* paths relevant to UHP behavior of tonalites. The bold line shows the tonalite vapor-absent solidus and (in italics) the phases that control the solidus over various pressure intervals. At pressures lower than 6–8 kbar and between 16 and 22 kbar, the tonalite solidus probably corresponds to the amphibole + quartz vapor-absent solidus (labeled VS01, after Vielzeuf & Schmidt, 2001). Biotite ± amphibole dehydration-melting defines the solidus between these two pressures. At pressures greater than ~22 kbar the tonalite vapor-absent solidus is defined by zoisite and phengite dehydration-melting reactions (see text). Other phase boundaries shown are: tonalite vapor-saturated solidus (LW74: Lambert & Wyllie, 1974; S93: Schmidt, 1993); inferred phengite + coesite + clinopyroxene vapor-absent solidus (HG01: Hermann & Green, 2001) and zoisite + coesite H_2O-saturated solidus (PS95: Poli & Schmidt, 1995). The dark grey area shows approximate *P–T* field over which tonalites are partially molten under vapor-absent conditions. The cross-hatched area shows approximate conditions at which subsolidus elimination of amphibole takes place in tonalites (see Fig. 7). The light grey area and arrow show the range of *P–T* paths identified in UHP metamorphic terranes, after Chopin (2003). 'Normal Moho' and 'deepest Moho' show approximate pressures at the bottom of 35 and 70 km deep continental crust, respectively.

of ~20–25 kbar, in response to the stabilization of a high-density, garnet-rich peritectic assemblage (e.g. Wyllie & Wolf, 1993; Vielzeuf & Schmidt, 2001). The negatively sloping amphibole + quartz solidus was not observed in the tonalite experiments, probably because reaction of amphibole under fluid-absent conditions is kinetically inhibited. Experimental evidence and theoretical arguments, however, strongly suggest that this part of the amphibole + quartz solidus is largely suppressed in tonalites. The reason for the dramatically different behaviors of amphibolites and tonalites is the presence of K-feldspar in the latter, which allows amphibole to be eliminated by means of water-conserving subsolidus reactions such as (7) and (8).

The phengite + coesite/quartz + clinopyroxene vapor-absent solidus of Herrmann & Green (2001), which corresponds to reaction (10) in the tonalite, was located by those workers at temperatures 100–150°C lower than those inferred for the tonalite (Figs 7 and 11). Their vapor-absent solidus, however, is based on an extrapolation of results of experiments with small amounts of added H_2O, which makes a direct comparison with vapor-absent experiments problematic. In addition, the natural tonalite starting material used for these experiments contains Ti, which was not present in Hermann & Green's synthetic compositions. Significantly, peritectic phengite in the tonalite melting experiments contains up to ~2 wt % TiO_2, which can have a powerful stabilizing effect on this phase. For these reasons, I argue that the UHP phengite solidus reported here is more appropriate to melting of dry tonalites in nature than the one proposed by Hermann & Green (2001).

THE FATE OF TONALITIC CRUST DURING CONTINENTAL SUBDUCTION

The experimental results presented here, together with previous work on vapor-present melting of tonalites,

provide a model for the fate of tonalitic crust during UHP metamorphism and continental subduction. If free H_2O is available, then the crust will melt during UHP metamorphism [Fig. 11; range of UHP decompression P–T paths from Chopin (2003)]. The dearth of evidence for partial melting in UHPM terranes, together with more general considerations about the behavior of hydrous fluids during high-grade metamorphism (e.g. Yardley & Valley, 1997) argues against water-rich conditions during continental subduction. Vapor-absent conditions are likely to constitute a more appropriate model for UHP metamorphism. Under such conditions, tonalitic crust remains unmolten during continental collision, subduction and exhumation (Fig. 11). There are a few possible exceptions. For example, UHP metamorphism in the Kokchetav massif (Kazakhstan) followed a hotter P–T path than in other areas of continental subduction. Shatsky *et al.* (1999) described trondhjemite veins, which might represent UHP melts, cutting across eclogite bodies. Trondhjemitic melt compositions are most closely approached in the 21 kbar experiments (Fig. 8), at which pressure melting of tonalites begins at temperatures of the order of 930°C, which is within the range of the Kokchetav massif's P–T path (e.g. Shatsky *et al.*, 1995).

More striking are sanidine eclogite crustal xenoliths from the Pamirs (Hacker *et al.*, 2003, and in preparation), which have mineral assemblages (omphacite + garnet + sanidine + kyanite + quartz) that are identical to those formed by UHP partial melting of tonalites. Thermobarometry of the sanidine eclogite xenoliths yields pressures in the range 20–27 kbar and temperatures of 1000–1100°C, in excellent agreement with the conditions at which their mineral assemblages can form by partial melting of tonalites (e.g. Figs 6 and 7). The existence of these xenoliths suggests that the hot conditions that are needed to cause UHP vapor-absent melting of supracrustal igneous or meta-igneous rocks are attained in nature in at least some instances of continental subduction. The fact that these very hot UHP crustal rocks have so far been found only as volcanic xenoliths and not among exhumed UHP metamorphic terranes is potentially very significant. It could mean that igneous continental crust can be exhumed after UHP metamorphism only if it never becomes hot enough to undergo substantial melting. If it does undergo partial melting and a minimum of 20–30% melt extraction, then the density of the ensuing residues may be too high to allow their return to crustal depths (Fig. 10). Slices of igneous continental crust that are subducted to mantle depths and undergo partial melting may thus remain in the mantle indefinitely. The tantalizing possibility exists that injection of continental material into the mantle during continental collisions is far more important than commonly thought.

Melting becomes increasingly likely at depths greater than about 100 km ($P \approx 27$ kbar), where the negatively sloping zoisite + K-feldspar dehydration-melting solidus could perhaps lead to 'compression-melting'. The silica-, alkali- and H_2O-rich melts that are formed by UHP tonalite dehydration-melting are likely to be highly reactive in the mantle environment and could thus constitute powerful metasomatizing agents. Even high-density residues from which 20–40% melt has been extracted could still be significant reservoirs of incompatible elements and volatiles (Table 9, Fig. 10). This is so because of the wide temperature interval that separates the solidus from the zoisite- and phengite-out boundaries (e.g. Figs 6 and 7). Partially dehydrated crustal slices could thus be sources of mantle metasomatism long after their initial subduction. This may supply the long-suspected link between ancient continental collisions and more recent eruption of magmas of extreme compositions in cratonic environments.

ACKNOWLEDGEMENTS

T. C. McCarthy and Charlie Fortner assisted with some of the experiments. Thoughtful reviews by Jörg Hermann and journal editor Dennis Geist were most helpful in improving the manuscript. This work was supported by NSF grant EAR-9725190.

REFERENCES

Barker, F. (1979). Trondhjemite: definition, environment and hypotheses of origin. In: Barker, F. (ed.) *Trondhjemites, Dacites and Related Rocks. Developments in Petrology 6*. Amsterdam: Elsevier, pp. 1–12.

Carroll, M. R. & Wyllie, P. J. (1990). The system tonalite–H_2O at 15 kbar and the genesis of calc-alkaline magmas. *American Mineralogist* **75**, 345–357.

Chopin, C. (1984). Coesite and pure pyrope in high-grade blueschists of the western Alps: a first record and some consequences. *Contributions to Mineralogy and Petrology* **86**, 107–118.

Chopin, C. (2003). Ultrahigh-pressure metamorphism: tracing continental crust into the mantle. *Earth and Planetary Science Letters* **212**, 1–14.

Ernst, W. G. (2001). Subduction, ultrahigh-pressure metamorphism, and regurgitation of buoyant crustal slices—implications for arcs and continental growth. *Physics of the Earth and Planetary Interiors* **127**, 253–275.

Hacker, B., Luffi, P., Lutkov, V., Minaev, V., Ratschbacher, L., Patiño Douce, A. E., Ducea, M., McWilliams, M. & Metcalf, J. (2003). Near-ultrahigh pressure processing of subducted continental crust: Miocene crustal xenoliths from the Pamirs. *Geological Society of America, Abstracts with Programs* **35(6)**.

Hermann, J. (2002). Experimental constraints on phase relations in subducted continental crust. *Contributions to Mineralogy and Petrology* **143**, 219–235.

Hermann, J. & Green, D. H. (2001). Experimental constraints on high pressure melting in subducted crust. *Earth and Planetary Science Letters* **188**, 149–168.

Hermann, J., Rubatto, D., Korsakov, A. & Shatsky, V. S. (2001). Multiple zircon growth during fast exhumation of diamondiferous,

deeply subducted continental crust (Kokchetav Massif, Kazakhstan). *Contributions to Mineralogy and Petrology* **141**, 66–82.

Kretz, R. (1983) Symbols for rock-forming minerals. *American Mineralogist* **68**, 277–279.

Lambert, I. B. & Wyllie, P. J. (1974). Melting of tonalite and crystallization of andesite liquid with excess water to 30 kilobars. *Journal of Geology* **82**, 88–97.

Liou, J. G., Zhang, R. Y., Ernst, W. G., Rumble, D. & Maruyama, S. (1998). High-pressure minerals from deeply subducted metamorphic Rocks. *Reviews in Mineralogy* **37**, 33–96.

Liou, J. G., Ernst, W. G. & Ogasawara, Y. (2002). Petrochemical and tectonic processes of UHP/HP terranes I: Preface. *International Geology Review* **44**, 765–769.

Massonne, H. J. (1995). Experimental and petrogenetic study of UHPM. In: Coleman R. G. & Wang X. (eds) *Ultrahigh Pressure Metamorphism*. Cambridge: Cambridge University Press, pp. 33–95.

Massonne, H. J. (1999). Experimental aspects of UHP metamorphism in pelitic systems**.** *International Geology Review* **41**, 623–638.

Morimoto, N. (1988) Nomenclature of pyroxenes. *Mineralogical Magazine* **52**, 535–50.

Patiño Douce, A. E. (1995). Experimental generation of hybrid silicic melts by reaction of high-Al basalt with metamorphic rocks. *Journal of Geophysical Research* **100**, 15623–15639.

Patiño Douce, A. E. (1996). Effects of pressure and H_2O content on the compositions of primary crustal melts. *Transactions of the Royal Society of Edinburgh: Earth Science* **87**, 11–21.

Patiño Douce, A. E. & Beard, J. S. (1994). H_2O loss from hydrous melts during fluid-absent piston-cylinder experiments. *American Mineralogist* **79**, 585–588.

Patiño Douce, A. E. & Beard, J. S. (1995). Dehydration-melting of biotite gneiss and quartz amphibolite from 3 to 15 kbar. *Journal of Petrology* **36**, 707–738.

Patiño Douce, A. E. & Beard, J. S. (1996). Effects of P, $f(O_2)$ and Mg/Fe ratio on dehydration-melting of model metagreywackes. *Journal of Petrology*, **37**, 999–1024.

Patiño Douce, A. E. & Harris, N. (1998). Experimental constraints on Himalayan anatexis. *Journal of Petrology* **39**, 689–710.

Patiño Douce, A. E. & Johnston, A. D. (1991). Phase equilibria and melt productivity in the pelite system: implications for the origin of peraluminous granitoids and aluminous granulites. *Contributions to Mineralogy and Petrology* **107**, 202–218.

Patiño Douce, A. E. & McCarthy, T. C. (1998). Melting of crustal rocks during continental collision and subduction. In: Hacker, B. R. & Liou, J. G. (eds) *When Continents Collide: Geodynamics and Geochemistry of Ultrahigh-Pressure Rocks*. Dordrecht: Kluwer Academic, pp. 27–55.

Poli, S. & Schmidt, M. W. (1995). H_2O transport and release in subduction zones: experimental constraints on basaltic and andesitic systems. *Journal of Geophysical Research* **100**, 22299–22314.

Schmidt, M. W. (1993). Phase relations and compositions in tonalite as a function of pressure: an experimental study at 650°C. *American Journal of Science* **293**, 1011–1060.

Schmidt, M. W. & Thompson, A. B. (1996). Epidote in calc-alkaline magmas: an experimental study of stability, phase relationships and the role of epidote in magmatic evolution. *American Mineralogist* **81**, 462–474.

Shatsky, V. S., Sobolev, N. V. & Vavilov, M. A. (1995). Diamond-bearing metamorphic rocks of the Kokchetav massif (Northern Kazakhstan). In: Coleman R. G. & Wang X. (eds) *Ultrahigh Pressure Metamorphism*. Cambridge: Cambridge University Press, pp. 427–455.

Shatsky, V. S., Jagoutz, E., Sobolev, N. V., Kozmenko, O. A., Parkhomenko, V. S. & Troesch, M. (1999). Geochemistry and age of ultrahigh pressure metamorphic rocks from the Kokchetav massif (Northern Kazakhstan). *Contributions to Mineralogy and Petrology* **137**, 185–205.

Skjerlie, K. P. & Patiño Douce, A. E. (2002). The fluid-absent partial melting of a zoisite-bearing quartz eclogite from 1·0 to 3·2 GPa; implications for melting in thickened continental crust and for subduction zone processes. *Journal of Petrology* **43**, 291–314.

Smith, D. C. (1984). Coesite in clinopyroxene in the Caledonides and its implications for geodynamics. *Nature* **310**, 641–644.

Stöckhert, B., Duyster, J., Trepmann, C. & Massone, H. J. (2001). Microdiamond daughter crystals precipitated from supercritical COH plus silicate fluids included in garnet, Erzgebirge, Germany. *Geology* **29**, 391–394.

Taylor, S. R. (2001). *Solar System Evolution. A New Perspective*, 2nd edn. Cambridge: Cambridge University Press.

Vielzeuf, D. & Montel, J. M. (1994). Partial melting of metagreywackes. 1. Fluid-absent experiments and phase relationships. *Contributions to Mineralogy and Petrology* **117**, 375–393.

Vielzeuf, D. & Schmidt, M. W. (2001). Melting relations in hydrous systems revisited: application to metapelites, metagreywackes and metabasalts. *Contributions to Mineralogy and Petrology* **141**, 251–267.

Wyllie, P. J. & Wolf, M. B. (1993). Amphibole dehydration-melting: sorting out the solidus. In: Prichard, H. M., Alabaster, T., Harris, N. B. W. & Neary, C. R. (eds) *Magmatic Processes and Plate Tectonics. Geological Society, London, Special Publications* **76**, 405–416.

Yardley, B. W. D. & Valley, J. W. (1997). The petrologic case for a dry lower crust. *Journal of Geophysical Research* **102**, 12173–12185.